Toward the Realization of Single-Photon Sources for Radiometry Applications at Room Temperature

Kee Suk Hong, *Member, IEEE*, Hee-Jin Lim, *Member, IEEE*, Dong Hoon Lee, *Member, IEEE*,
In-Ho Bae, *Member, IEEE*, Kwang-Yong Jeong, *Member, IEEE*, Christoph Becher, *Member, IEEE*,
Sejeong Kim, *Member, IEEE*, and Igor Aharonovich

Abstract— Single-photon sources based on single emitters, such as 2-D materials and impurities in diamond, are of great interest for many application fields, including quantum communication, quantum metrology, and quantum sensing. In photometry and radiometry, a single-photon source, having the ability to emit only one photon in a well-defined time and frequency domain, represents a promising candidate to realize a photon number-based primary standard for quantum radiometry. At the Korea Research Institute of Standards and Science (KRISS), we have realized three kinds of single-photon sources based on various single emitters at room temperature: silicon vacancy (SiV) in diamond, defects in gallium nitride (GaN), and vacancy in hexagonal boron nitride (hBN). We found common factors related to the relaxation times of the internal states that indirectly affect the photon number stability. We observed a high photon number stability in the GaN emitter due to faster relaxation times compared with the hBN emitter, which, on the other hand, produced high rates of photons per second ($>10^6$). Moreover, we demonstrate repeatable radiant flux measurements of a bright hBN single-photon emitter for a wide radiant flux range from a few tens of femtowatts to one picowatt.

Index Terms— Optical metrology, quantum radiometry, single-photon avalanche diode, single-photon emission.

Kee Suk Hong, Dong Hoon Lee, and In-Ho Bae are with the Korea Research Institute of Standards and Science, Daejeon 34113, Republic of Korea (e-mail: hongi2011@kriss.re.kr; dh.lee@kriss.re.kr; inhobae@kriss.re.kr).

Hee-Jin Lim is with the Quantum Technology Institute, Korea Research Institute of Standards and Science, Daejeon 34113, Republic of Korea (e-mail: heejin.lim@kriss.re.kr).

Kwang-Yong Jeong is with the Department of Physics, Jeju National University, Jeju-si 63243, Republic of Korea (e-mail: kyjeong83@gmail.com).

Christoph Becher is with the Naturwissenschaftlich-Technische Fakultät, Fachbereich Physik, Universität des Saarlandes, 66123 Saarbrücken, Germany (e-mail: christoph.becher@physik.uni-saarland.de).

Sejeong Kim is with the Department of Electrical and Electronic Engineering, University of Melbourne, Melbourne, VIC 3010, Australia (e-mail: Sejeong.kim@unimelb.edu.au).

Igor Aharonovich is with the School of Mathematical and Physical Sciences and the ARC Centre of Excellence for Transformative Meta-Optical Systems, University of Technology Sydney, Ultimo, NSW 2007, Australia (e-mail: Igor.Aharonovich@uts.edu.au).

Digital Object Identifier 10.1109/TIM.2023.3289550

I. INTRODUCTION

ADVANCED photon measurement with high repeatability and low uncertainty is the key element in few-photon metrology based on photon number [1], [2], [3], [4], [5], [6]. While low photon number fluctuations and high repeatability are important features for qualifying a standard light source, these can be limited by malicious phenomena, such as blinking and internal relaxations in single-photon emitters [7], [8], [9], to different degrees in different materials. In this study, we focus on materials that emit single-photon fluorescence at room temperature by investigating silicon vacancy (SiV) in diamond, defects in gallium nitride (GaN), and vacancy in hexagonal boron nitride (hBN) as spectrally narrow and accessible platforms. One of purpose we aimed in this work is to bridge between our classical system of detection efficiency calibration for single-photon detectors and its continuation based on single-photon source. The former calibration system was made for narrow-line wavelengths using continuous wave (CW) and classical light sources. However, CW-operated single-photon emission from a spectrally narrow line [10], [11] at room temperatures [12] to combine with the system is more sensitive to spectral diffusion and blinking phenomena [9], [13], which affect significantly in photon number uncertainty.

For details on sample preparation, see Appendix B. We characterize the photon number statistics and fluctuations of the emitters, since their degrees are major factors in determining the accuracy of photon flux for radiometry applications. In addition, we compare the maximum count rate allowed for the bare materials under the conventional collection technique of confocal microscopy. The reason why we stress this condition is that detection count rates are not intrinsic but rather depend on the efficiencies given by refractive index geometries and detection techniques. We note that the present experiments are limited by estimations of internal quantum efficiency and the theoretically maximum count rates under CW operation; more specific methods to optimize the collection efficiency, an important subject of photonics, remain for future, application-oriented studies.

To find general tendencies and characteristics from among the complexity and variety of our materials, this work was based on a large amount of data collected from numerous emitters. Our full dataset consists of two levels: the first concerns basic properties in identifying the single-photon emitters, and the second concerns figures of measurements
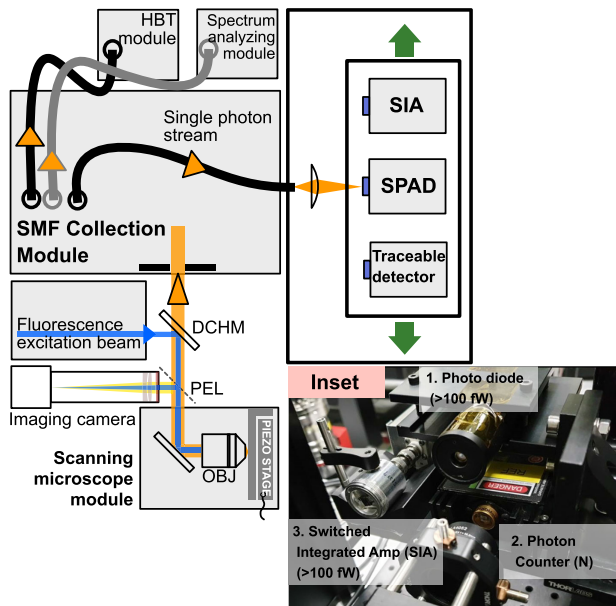
Fig. 1. Modular system for fluorescence-based single-photon generation. The inset is an image of three different detectors: 1—photodiode with fA amplifier (Keithley 6430), 2—SPAD (Excelitas), and 3—SIA (homemade).

for conversion to radiometry flux. Data fields in the first level are of photon coincidence correlation $g^{(2)}(0)$, spectra, and stability, which have been used to authenticate single-photon fluorescence. Statistical distributions of the positions of the spectral peaks were massively surveyed for collective studies on defect states and their formations. Following details of our methods in Section II, we discuss the results of these basic properties in Section III. Data fields in the second level of our dataset include measurements for conversion to radiometry flux. These are examined with a dual detection system that measures photon streams with two modes of detection, namely, photon counting detectors with results in count per second (cps) and a photocurrent-generating photodiode with results in joules per second (W). Having two different detection mechanisms enables a comparison of outcomes for the same single-photon stream as well as an examination of the uncertainty of conversion between the two measures. Setting the system to photon counting detection, we measured both the photon number fluctuation and repeatability of the photon flux measurements to evaluate the degrees of stability both for the photon sources and for the detection system itself, respectively. The analyzed results are discussed in Section IV, and our conclusion is given in Section V. This article is an extension of the proceedings paper [14], containing more details of material characteristics regarding blinking and stability.

II. EXPERIMENTAL METHOD

Confocal microscopes have been commonly used for investigating single-photon emitters dispersed in nanocrystals or randomly located in shallow depths of crystal. We were helped by the measurement system of our previous work, where we set up modules for single-photon collection with single-mode fibers (SMFs) and analyzed their photon number statistics [15].

The setup has benefits of uninterrupted serial measurements of spatial positions, spectra, and photon statistics $g^{(2)}(0)$, and a high stability of maintained alignments that leads to repeatable measurements (see Section III). The SMF interface gives identical beam profiles for analyzing the modules, leaving the external systems available for exploitation. The theoretically maximum collection efficiency from the sample–air interface to the SMF output via an objective lens of numerical aperture 0.95 and its matching fiber-collimation lens is 21%, assuming a Gaussian beam as in past work [15]. The collection efficiency, $<6.4\%$, was drawn with consideration of the mode coupling efficiency of electrical dipole radiation and SMF mode [16], [17] (for more details, see Appendix A). The real collection efficiency is smaller than this prediction, though, when we take into account surface scattering and all the variable nanocrystal shapes. Still, our photon count rate results are similar to other works that studied the same materials, implying a sufficient level of mechanical rigidity to maintain the count rate.

For the evaluation of photon number for application to radiometry experiments, we constructed a radiometry module that includes the dual detection system described above, a schematic of which is shown in Fig. 1. This new module has three stages of detection, as shown in the inset of Fig. 1: a traceable photodiode with fA amplifier (Keithley 6430), a silicon single-photon avalanche detector (SPAD; Excelitas) for photon flux counting, and a switched integrated amplifier (SIA; homemade) for output power indication [18]. All three share the same single-photon input injected via SMF and the same incidence position at which we rotate groups of detectors in place. The characteristics of room temperature single-photon light sources can be checked through each module. Finally, a separate output module was installed and compared with a traceable detector.

III. SINGLE-PHOTON EMITTER CHARACTERISTICS

The spectra of fluorescence centers commonly consist of a zero-phonon line (ZPL) and phonon sidebands, where there is a high ratio of ZPL intensity compared with the phonon sidebands, i.e., a high Debye–Waller factor [19], as shown in Fig. 2(a)–(c). The ZPL positions of hBN and GaN depend on strain and defect formations and are widely distributed over 600–750 and 690–800 nm, respectively [Fig. 2(d)].

Due to the different mechanisms of defect formation between GaN and hBN, GaN has a greater linewidth on average and can be more directly affected by crystal strain. Both GaN and hBN have a wide linewidth on average that can vary by the local strain of the host crystal because of the various kinds of defect formations and their large degrees of freedom. On the other hand, SiV has a definite ZPL position, ≈ 737 nm [20], the formation of which is explicitly allowed by the diamond crystal.

For a statistical approach, we collected photon statistics from >20 fluorescence emitters. Single-photon emitters have a unique property of fluorescence, exhibiting a low coincidence of photon count. The degree and time scale of this coincidence suppression have been commonly represented by the normalized correlation $g^{(2)}(\tau) = \langle C(t+\tau)C(t)\rangle / \langle C(t)\rangle^2$ of
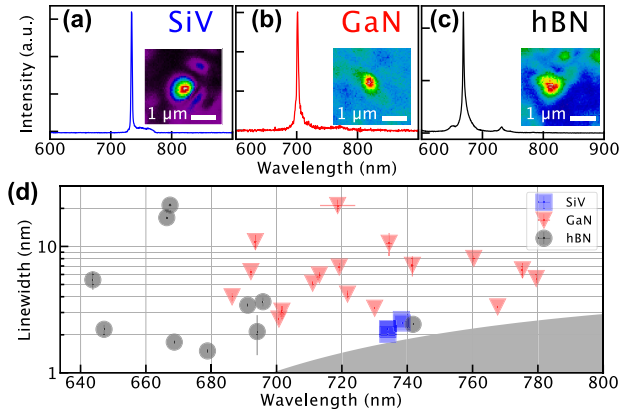
Fig. 2. Spectra of single-photon emitters of different materials. (a) SiV in diamond, (b) fluorescence defects in GaN crystal on a sapphire wafer (GaN), and (c) vacancy in hBN (hBN). Insets are images of photoluminescence from scans over the area of each fluorescence center. (d) Plots of the spectral peak center over a range of wavelength and linewidth for SiV (blue), GaN (red), and hBN (gray). The gray zone is the resolution boundary limited by our spectrometer and its coupling optics.

photon count rate (C) as measured by a Hanbury Brown–Twiss interferometer [21]. We employed two methods of deducing $g^{(2)}(\tau)$ experimentally: start–stop histogram and time-tag correlation (TTC). The former is advantageous for real-time acquisition, as the trigger intervals between signals from two SPADs are collected. The latter, though, has a better convergence at $g^{(2)}(\infty) \rightarrow 1$, because this method stores time tags and deduces a normalization factor from the total count number of each detector during data processing, which gives reliable results of $g^{(2)}(0)$. In our study, estimations of $g^{(2)}(\tau)$ were based on raw data from the TTC method. The $g^{(2)}(\tau)$ from our samples, however, shows composite features of both antibunching ($g^{(2)}(\tau) < 1$) at $|\tau| < \tau_1$ and bunching ($g^{(2)}(\tau) > 1$) at $\tau_1 < |\tau| < \tau_2$ simultaneously. Here, τ_1 and τ_2 are effective time constants defined by the fitting model $g^{(2)}(\tau) = 1 - p_1 e^{-|t|/\tau_1} + p_2 e^{-|t|/\tau_2}$, where p_1 is the depth contributing to the antibunching of $g^{(2)}(0)$, p_2 is the height above $g^{(2)}(\tau) > 1$, τ_1 is the time width of antibunching, and τ_2 is the characteristic exponential decay time of bunching. We collected τ_1 and τ_2, because they have physical origins: τ_1 is the spontaneous emission time for an ideal photon source, relating to the lifetime of the radiative transition for single-photon emission, while τ_2 stems from nonradiative relaxations, which can cause blinking in the photon emission [22]. If a single emitter is trapped in metastable dark states, it stops emitting until it is released to bright states, with τ_2 directly representing this time scale.

With this model, we observed $g^{(2)}(0) = 0.38 \pm 0.22$ for SiV, 0.24 ± 0.14 for GaN, and 0.33 ± 0.05 for hBN, as shown in Fig. 3(a)–(c), where the errors are the widths of the 95% confidence interval calculated via robust covariance estimation [23]. The full set of $g^{(2)}(0)$ data were measured from >20 fluorescence centers of our samples, as shown in Fig. 3(d). The large errors in the $g^{(2)}(0)$ obtained from the SiV emitters are due to the short τ_1 of these emitters and a time jitter of the detector. To restore the pure $g^{(2)}(0)$ before the time jitter noise, we tried a deconvolution method with a noise filter:
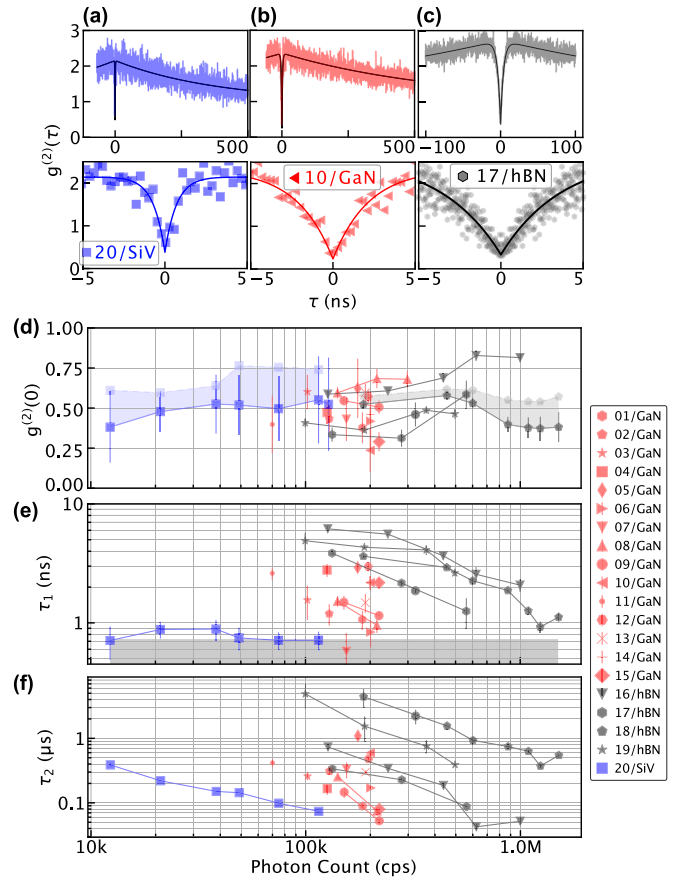

Fig. 3. Photon correlation $g^{(2)}(\tau)$ acquired from a Hanbury Brown–Twiss interferometer for (a) SiV in diamond (blue), (b) defects in GaN (red), and (c) vacancy in hBN (gray). Solid lines show the model $g^{(2)}(\tau) = 1 - p_1 e^{-|t|/\tau_1} + p_2 e^{-|t|/\tau_2}$ with characteristic times of antibunching (τ_1) and trapping in metastable dark states (τ_2). Fitted to this model, the zero-time correlations $g^{(2)}(0)$ are derived to be (a) 0.38 ± 0.22, (b) 0.24 ± 0.14, and (c) 0.33 ± 0.05 (95% confidence interval). From the full set of data attained from various fluorescence centers in the three materials, photon counts as acquired from the detectors are plotted for (d) $g^{(2)}(0)$, (e) τ_1, and (f) τ_2. The gray zone in (e) is the resolution boundary limited by the time jitter noise of the single-photon detectors.

$H(\tau; D) = (D\sqrt{2\pi})^{-1} \exp(-\tau^2/2D^2)$ assumed for time jitter $D = 0.3$ ns [24]. Our method of deconvolution is to fit the data with a convolution form of an exponential function. However, this method is redundant, as its results are similar to the previous estimation of $g^{(2)}(0)$ with parameters of p_1 and p_2, and the results can be biased when D is overestimated. It is a common tendency regardless of the material that time jitter errors of $g^{(2)}(0)$ grow as τ_1 is shortened. Since $g^{(2)}(\tau)$ measured by TTC is in absolute values, we could take the average $g^{(2)}(0)$ for some intervals of τ in $(-\tau_1, \tau_1)$. These experimentally allowed values are also presented as transparent points from the 18/hBN fluorescence emitter, as shown in Fig. 3(d). Their differences from the pure values $g^{(2)}(0)$ of the model are reflected in the confidence intervals for all emitters. Our closest recorded $g^{(2)}(0)$ values to 0 were attained around 0.24 ± 0.14 from GaN and 0.31 ± 0.05 from hBN, both of which are allowed at a low excitation power of CW 532 nm in wavelength. The excitation photon energy was chosen to be smaller than bandgap energies of materials, but greater than emission photon energies. The effective excitation power
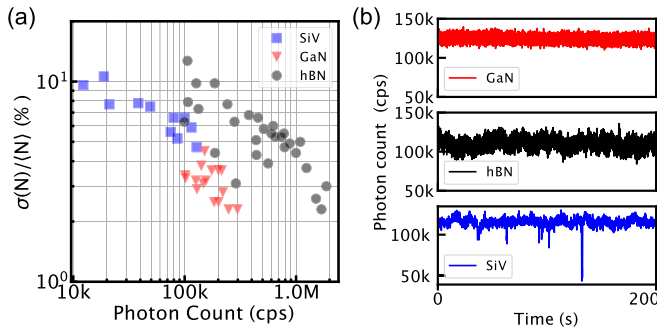
Fig. 4. (a) Standard deviation per average photon count number $\sigma(N)/\langle N \rangle$ as the stability error of the photon count number (N), acquired for 10 s with 10-ms time bins from various fluorescence centers of SiV (blue), GaN (red), and hBN (black). (b) Photon count rate with fluorescence emissions from defects in GaN (red), vacancy in hBN (black), and SiV (blue) over 200 s.

differed among materials and samples due to the differences in refractive index, diameter of grains, and geometry. However, the set of data used for Fig. 3(d)–(f) contains the full range of photon count rates achieved from far below and above the saturation points of each material. We suspect that the lowest value of $g^{(2)}(0) > 0.2$ can either be attributed to background photoluminescence, including deeper infrared, as we used a long pass filter with a 568-nm edge for purification, or the unresolved single-photon emitting transitions in a ZPL [25]. We discuss this in Section V.

Results show that τ_1 and τ_2 decrease with an increasing excitation power (P) for every material we observed. These variables of the $g^{(2)}(\tau)$ model have an origin in the relaxation processes of the fluorescence materials. The power dependence of τ_1 evidently shown with GaN and hBN implies that τ_1^{-1} represents a re-excitation rate rather than a spontaneous emission rate, under moderate levels of P allowing exploitable photon count rates. Nevertheless, we can expect large spontaneous emission rates from SiV, whose τ_1 is short, being close to the instrumental time jitter limit over the entire range of P. According to the three-level model, τ_2 is related to a recovering relaxation from metastable states (deshelving) and also depends on excitation power, because it gives more chances for initializing ionization [9], [22], [26]. We observed high count rates of $>10^6$ cps with hBN, similar to other studies [27], and low count rates of $<2 \times 10^5$ cps with SiV. This result is opposed to the long $\tau_{1,2}$ of hBN, as shown in Fig. 3(e) and (f), and to the intuition that fast transitions allow high photon rates. The speed of the transitions and blinking of SiV was the highest among the materials of interest, but exact pictures of these have yet to be unveiled to predict the internal efficiency of fluorescence emissions at room temperature [28], [29]. The photon count rate of GaN, $<3 \times 10^5$ cps, seems limited by the total internal reflections at the GaN–air interface, which can be overcome with an immersion medium before the objective lens. Otherwise, hBN is preferable for radiometry experiments that require a wide range of photon counts on the order of $>10^6$ cps.

Low photon number uncertainty is required for an ideal photon source. From various values of τ_2 depending on the emitters and materials, which are related to the time scales of

emission blinking, we can infer which ones have a low photon number fluctuation. We first measured the photon number uncertainty $\sigma(N)/\langle N \rangle$, defined as the ratio of the standard deviation of photon number [$\sigma(N)$] to its average value ($\langle N \rangle$). These statistical variables were obtained by a single shot of streaming acquisition of photon counts over 10 s. Photon number N is the accumulated photon count in a 10-ms-long time bin (Δt) within the streaming acquisition. The measured differences in uncertainty between the materials are shown in Fig. 4(a). The measured values of the uncertainty are split into two groups: SiV and hBN on one side, and GaN on the other side. With a few exceptions, every GaN emitter exhibited a smaller $\sigma(N)/\langle N \rangle$ than SiV and hBN. This can be readily seen from the real-time data in Fig. 4(b).

The main cause of large uncertainty of photon number is due to disturbance by relaxation to dark meta-stable internal states and to fast jumping movements of spectrum. From earlier reports, these could be observed at cryogenically low temperatures and even with resonant excitations [9], but their severity could be eased by passivation that removes electrostatic disturbance [13]. Theoretically, the performance of photon number stability should be explained by the density of internal states and inner process of random relaxation, proven that this dynamics were still remained at low temperatures [9]. However, in noisy environment of room temperatures (by a natural convection cooling of the constant air temperature 23 °C $\pm$ 0.5 °C), passivation seems to play the first role of protection for photon number stability. GaN defect emitters can benefit the passivation-like effect from their deep location formed near the GaN/sapphire epitaxy surface, and distant to air/GaN surface. Thermal collision can be the secondary cause of the phenomena. Epitaxially grown GaN on sapphire substrate has a greater speed of thermal drain (diffusivity) for a local heat possibly generated by laser absorption than SiV and hBN in powder forms, which can be advantageous to calm thermal fluctuations.

Compared with the existing radiometric standards, the stability of the single-photon sources ($\sim$2% in our best) is still inferior to that of the well-stabilized tungsten or laser sources, which shows a flux stability level of 0.01% expressed as the relative standard deviation. However, the single-photon sources provide the unique characteristics regarding the photon number statistics and avoid to use any attenuating element to bridge the large difference of the flux level.

IV. CONVERSION FROM PHOTON NUMBER TO OPTICAL POWER

In order to apply single-photon emitters in radiometry experiments, evaluations of the reliability of the measurement results are prerequisite. The main quality of our assessment is the repeatability of photon flux (Φ_q) or photon count rate (C) measurements followed by conversion to radiant flux (S). We performed two tests: one to deduce the repeatability errors of $\langle N \rangle$, and the other to confirm the validity of applying the present calibration parameters for photon counts to represent radiant fluxes. The dual detection module introduced in Section II is well suited for performing these tests. With this module, we measured C and S from an SPAD and photodiode,

respectively, and cross-checked the independent results with previously proven calibration parameters.

Despite a low fluctuation and high repeatability, the maximum C obtained from GaN has a lower limit around 2×10^5 cps [Fig. 3(d)–(f)]. This also limits the signal-to-noise ratio (SNR) to 22 for S measurements by a silicon photodiode having a noise equivalent power of 8.4 fW/Hz$^{1/2}$ and integrating photocurrents for 10 s [18], [30]. To take advantage of the high SNR of S and the wide range of flux levels shown in Fig. 5, we chose 18/hBN among the hBN emitters (see Fig. 3), whose maximum C was about 2×10^6 cps. We adjusted the level of C by the incidence power of CW 532-nm laser for excitation (P) before objective lens. C has a behavior following the function $C = C_0(1 - e^{-P/P_{sat}})$ with a saturation count rate of $C_0 = 1.8 \times 10^6$ cps and the power coefficient of excitation saturation $P_{sat} = 1.3$ mW. Note that the pump laser was out-focused to mitigate a sharp condition of pump-collection matching. We exploit the incidence power normalized by the saturation coefficient (P/P_{sat}) as an indicating parameter for the excitation strength. Over the wide range of C, $g^{(2)}(0)$ remained within the range 0.37–0.58. The uncertainty of $g^{(2)}(0)$ (95% confidence interval) increased at high C, as strong excitation power shortens the antibunching time width τ_1 to within the time jitter limit of the SPAD, as shown in Fig. 3(e).

As shown in Fig. 5(c), we obtained $g^{(2)}(0) = 0.53 \pm 0.03$ when measuring 18/hBN at a low excitation power of $0.15 \times P_{sat}$, and this value decreased to 0.35 at higher P. We attribute this irregularity to the presence of other transitions that independently emit single photons. Spectral investigations reveal that the ZPL is composed of two Lorentzian peaks, labeled 1 and 2 in Fig. 5(b). Similar findings were observed in another work, and according to the previous analysis, we can predict that cross correlations between independently emitted single photons increase $g^{(2)}(0)$ [25]. As the overlapped peaks 1 and 2 have mostly similar areas, the degree of mixture is sufficient to be the main cause of the high $g^{(2)}(0)$. We also attribute the oscillating behavior of $g^{(2)}(0)$ with respect to P to a property of mixture in which different excitation cross sections of fluorescence transitions make them compete in contributing to a sum of the photon count rate.

Because of the narrow linewidth ($\Delta \lambda \sim 2$ nm) shown in Fig. 5(b), we took a single value of detection efficiency at the center wavelength $\lambda_c = 665.8 \pm 0.03$ nm, with the justification that the efficiency deviation for wavelengths within the narrow line is smaller than the measured uncertainty (0.5%). Error caused by detection dead time and nonlinear counting was predicted to be 0.2% at $C = 10^5$ cps and to grow to 4% at $C = 5 \times 10^5$ cps, indicating that error correction is critical for $C > 10^5$ cps. For this, we used the correction function $C' = U(C)$ to present the corrected count rate, C', as defined in a previous work [30]. At this stage, with given quantum efficiency η, we can extract the important $\Phi_q = \eta \times C'$. In practice, we can reduce this to $\Phi_q = DE(C) \times C$ by introducing an effective detection efficiency function $DE(C)$ that includes both effects of η dependence and $U : C \to C'$. Note that $DE(C)$ was measured under consideration of the effect of deadtime and afterpulsing probability [30]. Then, we represent the relation
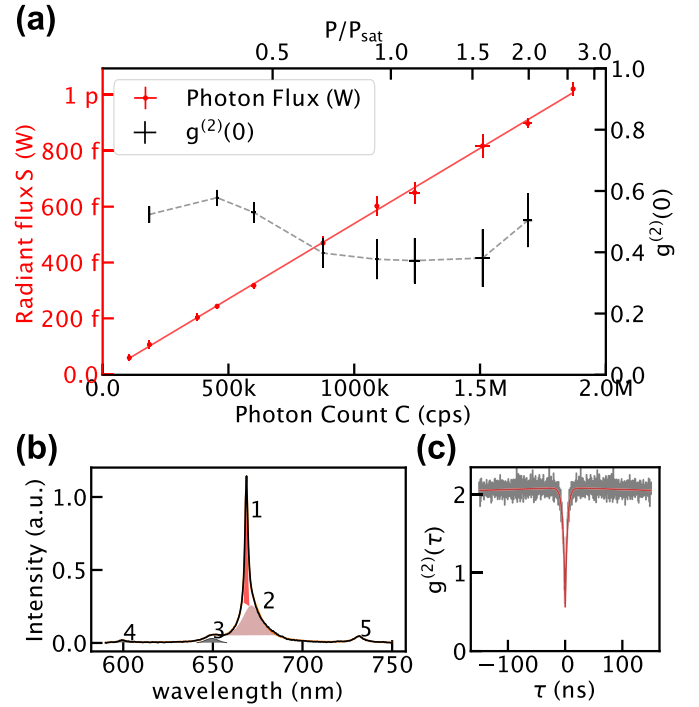

(a)

(b)

(c)

Fig. 5. (a) Relation between radiant flux (red dots) and photon count rate (C), where detections are based on different mechanisms of operation. The radiant fluxes (y-axis) are given by currents produced in a traceable, high-sensitivity photodiode, and the photon fluxes are from a single-photon counter (SPC). The solid red line represents the theoretical relation $S = (hc/\lambda)\eta\Phi_q$, identical to (1), where η is the quantum efficiency of the SPC, λ is the center wavelength, Planck constant h, and the speed of light c. The black dots show $g^{(2)}(0)$ varied at different levels of C. The laser power relative to the power coefficient of excitation saturation (P/P_{sat}) is presented to indicate the excitation strength. Horizontal bars are about standard deviation of measured C. (b) Spectrum of the single-photon source presents mainly as a Lorentzian function centered on 665 nm with a full width at half maximum (FWHM) of 2 nm in wavelength (1) while containing small peaks (2–5). (c) Photon autocorrelation measured at an excitation power of 0.2 mW and a photon count of 2×10^5 cps. All data were measured with 18/hBN (see Fig. 3).

between S and Φ_q in a convenient form with the uncorrected variable C, Planck constant h, and the speed of light c

$$S = \frac{hc}{\lambda} \times DE(C) \times C. \quad (1)$$

This relation with a given $DE(C)$ agrees well with the experimental S and C data shown in Fig. 5(a). We first note that the parameters given in previous works were applied here identically, even though the measurement system in this work was newly fashioned. Second, identical results were achieved even with a nonclassical light source that was not fully controlled, as this new source contained uncontrolled internal dynamics related to τ_2 and the blinking phenomenon. Such a photon source may reduce the repeatability of C due to a high $\langle \Delta N \rangle^2$, but it does not cause contradictions with the given parameters in $DE(C)$, because the parameters are central values.

V. CONCLUSION

We have studied single-photon emitters based on fluorescence defects in various crystal materials at room temperature. SiV in diamond, defects in GaN, and vacancy in hBN platforms all have a narrow linewidth, and their spectral centers

are spread over a wide range of wavelengths. This is, in fact, an important advantage for few-photon radiometry where there exist various quantum efficiencies as variable parameters in conversion models for radiant power. Both stability and brightness are important qualities of single-photon sources in few-photon metrology. None of the materials investigated in this study are endowed with both characteristics simultaneously. For example, although single-photon sources in hBN nanoflakes exhibit high rates of photon detection, they are interrupted by slow blinking, which causes severe fluctuations in photon count rates. On the other hand, those in GaN show a high degree of stability and a high repeatability of emission rate, but their photon count rates are lower than those attained from hBN. Such differences can be expected from their shapes. Emitters in hBN are close to the surface or edges in a nanoflake, where electrostatic fields can have large effects and cause vulnerability to charge fluctuations. The phenomenon of severe blinking in hBN is also supported by a recent study that revealed many internal states and frequent relaxations between them, even at low temperature. On the other hand, emitters in GaN are embedded at a depth of a few micrometers, and this reduces the fluctuations caused by electrostatic fields. However, the flat surface with high refractive index of GaN significantly decreases its photon collection efficiency, according to the total internal reflection effect [31]. Various methods have been developed to alleviate total internal reflection. This has long been a subject to mitigate the surface effects in solar cells and light-emitting diodes, and many techniques have been developed. The simplest solution is a solid immersion lens that includes various lens techniques, such as micro-half-spheres and metasurfaces. These methods do not modify the regions near the emitters beneath the surface. We expect high collection efficiencies as supported by these methods, which will enable us to apply nonclassical photon number statistics, such as the one corresponding to the Fock state, and to achieve a high degree of number uncertainty.

APPENDIX A
COUPLING EFFICIENCY OF RADIATION FROM A POINT DIPOLE SOURCE TO A SINGLE-MODE OPTICAL FIBER

We assume an electric dipole source laid at a focal point in air and perpendicular to the cylindrical symmetry axis connecting an objective lens and an SMF collimation lens. Electromagnetic fields that refocused by the SMF collimation lens were analytically calculated from the Green dyadic function, while the ratio of the field intensity collected through a finite numerical aperture 0.95 (η_{NA}) was extracted [16]. Because the refocused field has a different profile from ab SMF mode, the field-to-field coupling efficiency (η_{SMF}) is <73.7% calculated using an inner product defined in [17]. Then, $\eta_{NA} \times \eta_{SMF} = 32\%$. Considering a setup loss of 20%, the overall efficiency excluding unknown substrate losses is reduced to 6.4%.

APPENDIX B
SAMPLE PREPARATION

The SiV sample was nanodiamonds on an iridium substrate grown to the shape of a film by a silicon-free chemical vapor deposition (CVD) process and milled to the diameters of 50–100 nm. Silicon was implanted after the clean CVD process to attain a high SiV purity [32]. The GaN sample was a commercially available four GaN crystal grown on a sapphire wafer [33]. Fluorescence centers in GaN are explained to be charge-trapped dots located at the intersection of a lattice dislocation stemming from the sapphire–GaN interface and a layer mismatch of crystal orientation, similar to a point-like potential wall in a 2-D quantum well [8]. The hBN sample was in the form of nanoflakes dispersed in an oxidized layer of silicon substrate. The nanoflakes are commercially available but required a special treatment of annealing in an inert environment: 800 °C for 30 min in Ar gas of 1-Torr pressure [34].

REFERENCES

[1] W. Tittel and G. Weihs, "Photonic entanglement for fundamental tests and quantum communication," *Quantum Inf. Comput.*, vol. 1, no. 2, pp. 3–56, Aug. 2001.

[2] S. Chen et al., "Deterministic and storable single-photon source based on a quantum memory," *Phys. Rev. Lett.*, vol. 97, no. 17, Oct. 2006, Art. no. 173004.

[3] R. C. Willson, "Active cavity radiometer," *Appl. Opt.*, vol. 12, no. 4, p. 810, Apr. 1973.

[4] J. E. Martin, N. P. Fox, and P. J. Key, "A cryogenic radiometer for absolute radiometric measurements," *Metrologia*, vol. 21, no. 3, pp. 147–155, Jan. 1985.

[5] J. Y. Cheung et al., "The quantum candela: A re-definition of the standard units for optical radiation," *J. Modern Opt.*, vol. 54, nos. 2–3, pp. 373–396, Jan. 2007.

[6] J. C. Zwinkels, E. Ikonen, N. P. Fox, G. Ulm, and M. L. Rastello, "Photometry, radiometry and 'the candela': Evolution in the classical and quantum world," *Metrologia*, vol. 47, no. 5, pp. 15–32, Aug. 2010.

[7] C. J. Chunnilall, I. P. Degiovanni, S. Kuck, I. Muller, and A. G. Sinclair, "Metrology of single-photon sources and detectors: A review," *Opt. Eng.*, vol. 53, no. 8, Jul. 2014, Art. no. 081910.

[8] A. M. Berhane et al., "Bright room-temperature single-photon emission from defects in gallium nitride," *Adv. Mater.*, vol. 29, no. 12, 2017, Art. no. 1605092.

[9] K. Konthasinghe et al., "Rabi oscillations and resonance fluorescence from a single hexagonal boron nitride quantum emitter," *Optica*, vol. 6, no. 5, p. 542, May 2019.

[10] A. Vaigu et al., "Experimental demonstration of a predictable single photon source with variable photon flux," *Metrologia*, vol. 54, no. 2, p. 218, Mar. 2017.

[11] P. Lombardi et al., "A molecule-based single-photon source applied in quantum radiometry," *Adv. Quantum Technol.*, vol. 3, no. 2, Feb. 2020, Art. no. 1900083.

[12] B. Rodiek et al., "Experimental realization of an absolute single-photon source based on a single nitrogen vacancy center in a nanodiamond," *Optica*, vol. 4, no. 1, pp. 71–76, Jan. 2017.

[13] X. Li et al., "Nonmagnetic quantum emitters in boron nitride with ultranarrow and sideband-free emission spectra," *ACS Nano*, vol. 11, no. 7, pp. 6652–6660, Jul. 2017.

[14] K. S. Hong, H.-J. Lim, D.-H. Lee, and K.-Y. Jeong, "Single photon sources for radiometry applications at room temperature," in *Proc. Conf. Precis. Electromagn. Meas.*, Wellington, New Zealand, Dec. 2022, p. 56477X.

[15] H.-J. Lim, K.-Y. Jeong, D.-H. Lee, and K. S. Hong, "Modular system for fluorescence-based single photon generation using a retro-reflector," *Opt. Mater. Exp.*, vol. 9, no. 12, p. 4644, Dec. 2019.

[16] L. Novotny and B. Hecht, *Principles of Nano-Optics*, 2nd ed. Cambridge, U.K.: Cambridge Univ. Press, 2012, ch. 3.

[17] P.-I. Schneider, N. Srocka, S. Rodt, L. Zschiedrich, S. Reitzenstein, and S. Burger, "Numerical optimization of the extraction efficiency of a quantum-dot based single-photon emitter into a single-mode fiber," *Opt. Exp.*, vol. 26, no. 7, p. 8479, Apr. 2018.

[18] S. Park, K.-S. Hong, and W.-S. Kim, "Switched integration amplifier-based photocurrent meter for accurate spectral responsivity measurement of photometers," *Appl. Opt.*, vol. 55, no. 9, p. 2285, Mar. 2016.

[19] A. Sajid, M. J. Ford, and J. R. Reimers, "Single-photon emitters in hexagonal boron nitride: A review of progress," *Rep. Prog. Phys.*, vol. 83, no. 4, Mar. 2020, Art. no. 044501.

[20] J. P. Goss, R. Jones, S. J. Breuer, P. R. Briddon, and S. Öberg, "The twelve-line 1.682 eV luminescence center in diamond and the vacancy-silicon complex," *Phys. Rev. Lett.*, vol. 77, no. 14, pp. 3041–3044, Sep. 1996.

[21] R. Loudon, *The Quantum Theory of Light*. Oxford, U.K.: Clarendon Press, 1973.

[22] C. Santori, D. Fattal, J. Vuckovic, G. S. Solomon, E. Waks, and Y. Yamamoto, "Submicrosecond correlations in photoluminescence from InAs quantum dots," *Phys. Rev. B, Condens. Matter*, vol. 69, no. 20, May 2004, Art. no. 205324.

[23] K. Sidik and J. N. Jonkman, "A comparison of the variance estimation methods for heteroscedastic nonlinear models," *Statist. Med.*, vol. 35, no. 26, pp. 4856–4874, Nov. 2016.

[24] M. Nomura, N. Kumagai, S. Iwamoto, Y. Ota, and Y. Arakawa, "Laser oscillation in a strongly coupled single-quantum-dot-nanocavity system," *Nature Phys.*, vol. 6, no. 4, pp. 279–283, Apr. 2010.

[25] A. Bommer and C. Becher, "New insights into nonclassical light emission from defects in multi-layer hexagonal boron nitride," *Nanophotonics*, vol. 8, no. 11, pp. 2041–2048, Nov. 2019.

[26] G. V. Astakhov and V. Dyakonov, "Defects for quantum information processing in SiC,"in *Defects in Advanced Electronic Materials and Novel Low Dimensional Structures*, J. Stehr, I. Buyanova, and W. Chen, Eds. Cambridge, U.K.: Woodhead, 2018, p. 211, doi: 10.1016/B978-0-08-102053-1.00008-9.

[27] M. Nguyen et al., "Nanoassembly of quantum emitters in hexagonal boron nitride and gold nanospheres," *Nanoscale*, vol. 10, no. 5, pp. 2267–2274, 2018.

[28] E. Neu et al., "Narrowband fluorescent nanodiamonds produced from chemical vapor deposition films," *Appl. Phys. Lett.*, vol. 98, no. 24, Jun. 2011, Art. no. 243107.

[29] S. Lindner et al., "Strongly inhomogeneous distribution of spectral properties of silicon-vacancy color centers in nanodiamonds," *New J. Phys.*, vol. 20, no. 11, Nov. 2018, Art. no. 115002.

[30] I.-H. Bae et al., "Detection efficiency measurement of single photon avalanche photodiodes by using a focused monochromatic beam tunable from 250 nm to 1000 nm," *Metrologia*, vol. 56, no. 3, May 2019, Art. no. 035003.

[31] S. R. Bowman et al., "Broadband measurements of the refractive indices of bulk gallium nitride," *Opt. Mater. Exp.*, vol. 4, no. 7, p. 1287, Jul. 2014.

[32] E. Neu et al., "Single photon emission from silicon-vacancy colour centres in chemical vapour deposition nano-diamonds on iridium," *New J. Phys.*, vol. 13, no. 2, Feb. 2011, Art. no. 025012.

[33] *The Film (2-μm P-Type/2-μm Undoped) Grown on Sapphire*, Supplied Suzhou Nanowin Sci. Technol. Co., Ltd, Suzhou, China, 2023. [Online]. Available: http://en.nanowin.com.cn

[34] T. T. Tran et al., "Robust multicolor single photon emission from point defects in hexagonal boron nitride," *ACS Nano*, vol. 10, no. 8, pp. 7331–7338, Aug. 2016.

Kee Suk Hong (Member, IEEE) received the B.S. degree in physics from Sogang University, Seoul, South Korea, in 2003, and the Ph.D. degree in physics from the Korea Advanced Institute of Science and Technology (KAIST), Daejeon, South Korea, in 2010.

Since 2011, he has been with the Korea Research Institute of Standards and Science (KRISS), Daejeon, where he is currently a Principal Research Scientist. His current research interests include single-photon source, single-photon detection, and quantum radiometry.

Hee-Jin Lim (Member, IEEE) received the B.S. and Ph.D. degrees in physics from the Korea Advanced Institute of Science and Technology (KAIST), Daejeon, South Korea, in 2008 and 2016, respectively, with a focus on developing a bright single-photon source.

He had joined the Quantum Spin Dynamics Laboratory, University College London, London, U.K., where he studied spectroscopy techniques for spin resonance measurements until 2017. He has been a Research Scientist with the Korea Research Institute of Standards and Science (KRISS), Daejeon, since 2018. His major research interests include spectroscopy of photon-emitting spin ensembles and single register both with microwave and optical techniques, and finally converged to hybridization of quantum microwave circuitry.

Dong Hoon Lee (Member, IEEE) received the M.S. and Ph.D. degrees in physics from the University of Kaiserslautern, Kaiserslautern, Germany, in 1997 and 2000, respectively.

Since 2003, he has been with the Korea Research Institute of Standards and Science (KRISS), Deajeon, South Korea, where he is currently a Principal Research Scientist. His current research interests include optical radiometry, single-photon radiometry, laser radiometry, and characterization of optical detectors.

In-Ho Bae (Member, IEEE) received the B.S., M.S., and Ph.D. degrees from Pusan National University, Busan, South Korea, in 2005, 2008, and 2012, respectively, all in physics.

Since 2014, he has been with the Korea Research Institute of Standards and Science (KRISS), Deajeon, South Korea, where he is currently a Principal Research Scientist. His current research interests include Rydberg atom-based quantum sensor, single-photon radiometry, and absolute cryogenic radiometer.

Kwang-Yong Jeong (Member, IEEE) received the B.S. and Ph.D. degrees in physics from the Korea Advanced Institute of Science and Technology (KAIST), Daejeon, Republic of Korea, in 2006 and 2012, respectively.

He has been an Assistant Professor with the Department of Physics, JeJu National University, Jeju-si, Republic of Korea, since 2021. His research interests include the nanophotonics and quantum photonics.

Christoph Becher (Member, IEEE) received the Ph.D. degree in physics from the University of Kaiserslautern, Kaiserslautern, Germany, in 1998.

He held two post-doctoral positions at the University of California at Santa Barbara, Santa Barbara, CA, USA (first demonstration of single-photon emission from semiconductor quantum dots); and the University of Innsbruck, Innsbruck, Austria (first quantum gate and cavity quantum electro-dynamics (QED) with trapped ions). He is currently a Full Professor of physics with Saarland University, Saarbrücken, Germany, where he has been leading the Quantum Optics Research Group since 2005. His current research interests include the field of quantum technologies for quantum communication and sensing, in particular exploration of color centers in diamond as quantum bits and single-photon nonlinear optics, e.g., quantum frequency conversion.

Sejeong Kim (Member, IEEE) received the Ph.D. degree in physics from the Korea Advanced Institute of Science and Technology (KAIST), Daejeon, South Korea, in 2014.

She was a Research Fellow with the University of Technology Sydney (UTS), Ultimo, NSW, Australia. She is currently a Lecturer with the University of Melbourne, Melbourne, VIC, Australia. Her research interests include exploring light–matter interaction at the nanoscale, particularly using optical/plasmonic cavities.

Igor Aharonovich received the Ph.D. degree from the University of Melbourne, Melbourne, VIC, Australia, in 2010.

He moved to Harvard for two years of post-doctoral training. He is currently a Professor with the University of Technology Sydney, Ultimo, NSW, Australia. His main contributions include discovery of new color centers in diamond and hexagonal boron nitride, and the development of new methodologies to engineer nanophotonic devices from these materials.